Article

Solid State Phosphorescence Enhancement of Pt^{II}-Based Emitters via Combination of π-Hole(Isocyano Group)··· d$_z^2$[Pt^{II}] and I···Cl Halogen-Bonding Interactions

Svetlana A. Katkova *[iD], Elina V. Antonova [iD], Anna M. Cheranyova [iD], Daniil M. Ivanov and Mikhail A. Kinzhalov [iD]

St Petersburg State University, 7/9 Universitetskaya Emb., Saint Petersburg 199034, Russia;
m.kinzhalov@spbu.ru (M.A.K.)
* Correspondence: s.katkova@spbu.ru

Abstract: The Pt^{II} isocyanide complex [Pt(ppy)Cl(CNC$_6$H$_4$-C≡C-Ph)] (**1**, Hppy=2-phenylpyridine) was co-crystallized with 1,4-diiodotetrafluorobenzene (1,4-DITFB), yielding **1**·1/2(1,4-DITFB) adduct. The I···Cl halogen-bonding and π-π-stacking interactions combined with the rare π-hole(isocyano group)···d_z^2[Pt^{II}] interactions were identified via analysis of X-ray diffraction data of the co-crystals. These two types of structure-determining interactions supplemented each other, and the system of I···Cl and π-hole(isocyano group)···d_z^2[Pt^{II}] contacts achieved a 1D extended ladder-type architecture. The density functional theory calculations, employing a set of computational tools, verified the role of I···Cl and π-hole(isocyano group)···d_z^2[Pt^{II}] noncovalent bonds in the spectrum of noncovalent forces. The solid-state photophysical study revealed an amplification of luminescence intensity in the co-crystals, which is attributed to the suppression of the nonradiative relaxation pathways due to an increase in the rigidity of the chromophore center.

Keywords: isocyanide ligands; π-hole interactions; noncovalent interactions; halogen bonding; luminescence; platinum(II) complexes

1. Introduction

Luminescent materials based on complexes of transition metals are a subject of rapidly growing interest due to their applications in the design and fabrication of lighting devices [1–7], chemosensors [8–10], and photocatalysts [11–14]. The strong spin-orbit coupling induced by the heavy atom effect facilitates both fast intersystem crossing and formal spin-forbidden triplet radiative decay [15–17], which conventionally explains the efficient transition metal species phosphorescence at room temperature (RT). The emission color and efficiency of these species are primarily determined by the choice of metal center and organic ligands (photophysical properties of platinum(II) phosphors have been analyzed in reviews [15,17–21]); in the solid state, photophysical properties are also intimately associated with their molecular conformations and crystal packing, which is determined through their intermolecular interactions [22–24]. In comparison with the covalent bonds, the intermolecular noncovalent interactions are in general locally weak; however, despite their low energy, in many cases these interactions can collectively play a dominant role in the formation of crystal packing. In contrast to octahedral d^6-Ru^{II} and d^6-Ir^{III} complexes, the open axial coordination sites of the square planar d^8-Pt^{II}-based species mitigate noncovalent binding to Pt^{II} centers. These noncovalent linkages can significantly modify both ground- and excited-state properties of Pt^{II}-based systems and, hence, the photophysical features [18,25–29]. Thus, the change in the nature of the excited state from MLCT to MMLCT [30–34] occurring with the formation of the metallophilic interactions leads to emission profile alterations and red-shifting radiation. At the same time, aggregation due to other contacts, e.g., hydrogen, halogen, chalcogen bonding, etc., generally leads to no change in emission color, but it can be followed by a quantum yield enhancement in

luminescence [35–39].

One of the successful approaches to obtaining improved crystalline forms of luminescent complexes is the preparation of co-crystals [40]. In co-crystal, molecules of diverse types alternate in such a way that the overall structure is described by a unit cell, in which strictly definite positions occupy certain types of molecules. Representative examples of such targeted use of noncovalent interactions to create phosphors with improved emission characteristics based on co-crystals of cyclometallated platinum(II) complexes are shown in Figure 1.

Sivchik, 2015; C–I•••Cl HaB

30-fold increase in the Φ_{em}

Katkova, 2021; C–I•••Cl HaB & $\pi h(C_6F_5I)\cdots d_z^2[Pt]$

2-fold increase in the Φ_{em}

Rozhkov, 2020; $\pi h(C_{10}F_8)\cdots d_{zz}[Pt]$

3.5-fold increase in the Φ_{em}
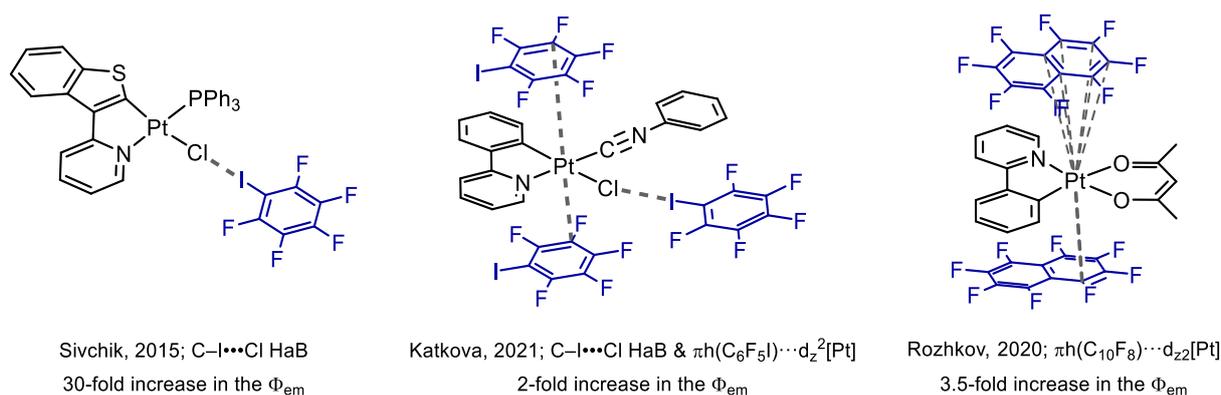
Figure 1. Examples of the directed use of nonvalent interactions for the creation of metal phosphors with improved emission characteristics based on adducts of cyclometallated platinum(II) complexes [35,37,41].

Among the wide variety of luminescent Pt^II-based systems, square planar cyclometallated complexes [Pt(C^N)XY] containing isocyanide ligands are of particular interest [42–47]. On the one hand, these ligands are strong field ligands that enhance luminescence efficiency at room temperature due to the destabilization of unoccupied *d* orbitals and the corresponding ^{3}MC states increasing a nonradiative pathway of excited-state relaxation [42]. Their luminescence has been attributed to the phosphorescence from the lowest triplet ligand-centered (^{3}LC) states perturbed by higher-lying singlet and triplet metal-to-ligand charge transfer (^{1,3}MLCT) states. On the other hand, the structure of isocyanide ligands can be modified with various substituents with different electron donor and steric properties, which influence the crystal packing on the complexes due to short- and long-range intermolecular interactions, as well as their photophysical properties [48]. In the context of this work, recent examples of photophysical modulations in cyclometallated Pt^II complexes with isocyanide ligands deserve separate consideration. Sicilia et al. reported a series of chloride/isocyanide [49] and alkynyl/isocyanide [50] cyclometallated Pt^II complexes in which the different electronic and steric effects of the CNR groups affected the crystal packing through short- and long-range Pt⋯Pt and/or π⋯π interactions and the photophysical properties. It was also recently reported that (isocyano group)⋯Pt^II interactions can influence photophysical characteristics [29]. We previously reported that the co-crystallization of [Pt(ppy)Cl(CNR)]-type complexes with X-^FArenes can leads to an increase in the quantum yield of luminescence with retention of the emission wavelengths [37].

In view of our general interest in luminescent transition metal complexes [51–54] and various applications of noncovalent interactions [37,52,55–58], in this work, using the example of cyclometallated Pt^II complex with aryl isocyanide ligand [Pt(ppy)Cl(CNC6H4-C≡C-Ph)] (1, Hppy=2-phenylpyridine), we recognized the ability to form co-crystallized adduct with 1,4-diiodotetrafluorobenzene (1,4-DITFB), in which the halogen-bonding I⋯Cl and the π-hole(isocyano group)⋯d_z^2[Pt^II] interactions were observed and studied using MEP surface analysis, a noncovalent interaction plot (NCI plot), the quantum theory of atoms in molecules (QTAIM), and the electron localization function (ELF).

2. Materials and Methods

2.1. Reagents, Instrumentation, and Methods

Solvents $K_2[PtCl_4]$ and 2-phenylpyridine (ppyH) were obtained from commercial sources and used as received. $[\{Pt(ppy)(\mu\text{-}Cl)\}_2]$ was prepared from $K_2[PtCl_4]$ and ppyH following the procedure in the literature [59]. Complex **1** was synthesized via the procedure in the literature [60]. UV-VIS spectra were measured with a Shimadzu UV-2550 spectrophotometer. The excitation and emission spectra in the solid state were recorded with a HORIBA FluoroMax-4 spectrofluorometer. The excited-state lifetimes and absolute photoluminescence quantum yields in the solid phase were measured with a HORIBA Scientific FluoroLog-3 spectrofluorometer using a HORIBA Quanta-phi integration sphere. The uncertainty of the quantum yield determinations was in the range of $\pm 5\%$ (an average of three replications, each of which was carried out with different orientations of the sample).

2.2. X-Ray Diffraction Study

Crystals of **1**·1/2(1,4-DITFB) were obtained by slow evaporation of an MeCN solution of a mixture of the corresponding isocyanide complex and 1,4-DITFB taken in a 1:2 molar ratio at 20–25 °C. A single-crystal X-ray diffraction experiment was carried out on a SuperNova, single source at offset/far, HyPix3000 diffractometer with monochromated CuKα radiation. The crystal was kept at 100(2) K during data collection. The structures were resolved by ShelXT [61] (structure solution program using intrinsic phasing) and refined by means of the ShelXL [62] program incorporated into the OLEX2 program package [63]. The crystallographic details are summarized in Table S1. Empirical absorption correction was applied in the CrysAlisPro (Agilent Technologies, Yarnton, UK, 2012) program complex using the spherical harmonics implemented in the SCALE3 ABSPACK scaling algorithm. CCCDC number 2,290,328 contains the supplementary crystallographic data for this paper. These data can be obtained free of charge from the Cambridge Crystallographic Data Centre via www.ccdc.cam.ac.uk/data_request/cif (accessed on 23 August 2023).

2.3. Computational Details

Calculations based on the experimental X-ray geometries of dimeric clusters were carried out at the DFT level [64–66] of theory using the dispersion-corrected PBE-D3 functional [67–69] (basis set def2-TZVP [70,71]) with the help of the Gaussian-09 program package [72]. The MEP surfaces of the clusters were presented using 0.001 a.u. isosurfaces [73,74]. The color scheme was a blue–green–red scale, with red for $\rho+$ cut (repulsive) and blue for $\rho-$ cut (attractive). Green isosurfaces corresponded to weakly repulsive and attractive interactions. The 3D surfaces and 3D visualizations of the NCI plot [75] with an isovalue = 0.35–0.4 and color scale data range of [–0.01; 0.01] were visualized using the VMD 1.9.3 program [76]. ELF projections [77] with the QTAIM method developed by Bader [78–81] were performed and presented in the Multiwfn 3.8 software [73]. The 1D profiles of the ED/ESP functions [82,83] were calculated in the Multiwfn program. Views of dimeric clusters were created using Chemcraft [84]. The BSSE-corrected interaction energies were calculated by subtracting the sum of the energies of the monomeric species from the total energy of the assembly.

3. Results

3.1. General Description of the X-Ray Structures

The crystallization of [Pt(ppy)Cl(CNC$_6$H$_4$-C≡C-Ph)] and 1,4-DITFB from MeCN solutions at RT was found to lead to **1**·1/2(1,4-DITFB) adduct (Figure 1). Only one type of crystal was obtained despite significant variation in the crystallization conditions (e.g., temperature, rate of evaporation). The peak position of the experimental PXRD pattern from solids obtained by solvent evaporation of a solution of a mixture of **1** and 1,4-DITFB taken in a 1:2 molar ratio matched well with the simulated PXRD pattern obtained from the

single-crystal X-ray structure **1**·1/2(1,4-DITFB), confirming the homogeneity of the sample and ruling out the presence of another phase (Figure S1.4, see Supplementary Materials).

The XRD analysis revealed that the asymmetric unit had one half of a 1,4-DITFB molecule in an inversion center and one molecule of complex **1** in a general position in the monoclinic co-crystal **1**·1/2(1,4-DITFB) (Figure 2, see Supplementary Materials, Figure S1.1, Table S1.2).
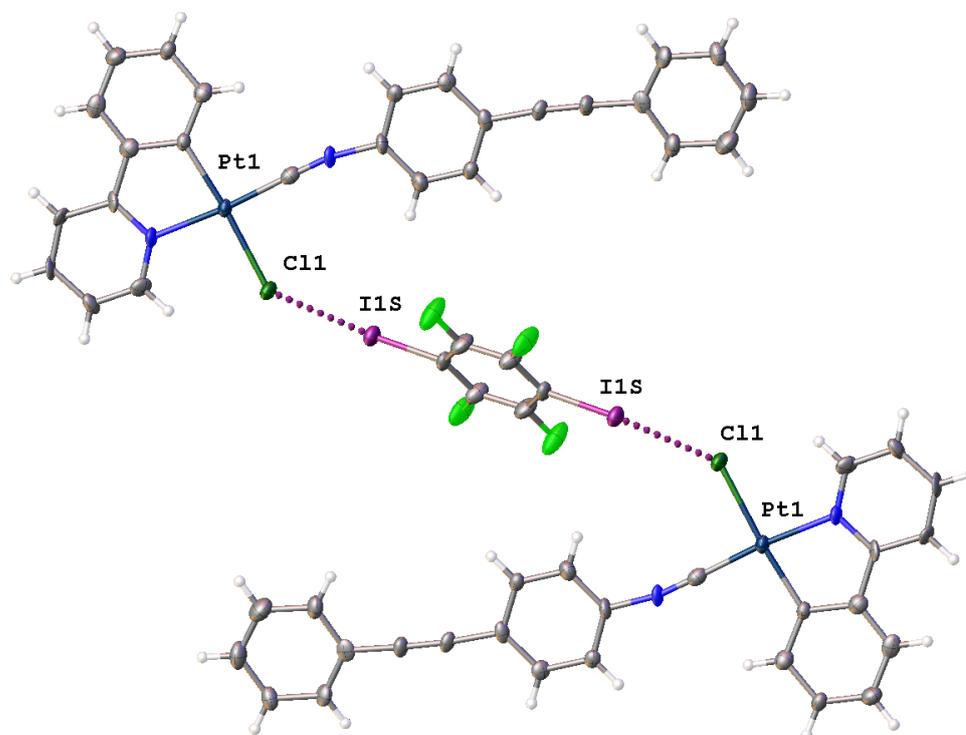
Figure 2. I···Cl HaB identified in the crystal structure of **1**·1/2(1,4-DITFB). Purple dotted line indicates the Pt–Cl···I–C HaBs.

The Pt atom of complex **1** exhibited distorted planar geometry similar to that reported for other [Pt(ppy)Cl(CNR)] complexes [29,37,51,52,60,85]. In **1**·1/2(1,4-DITFB), neighboring molecules of complex **1** showed weak stacking interactions between chelate and aromatic rings and π-π stacking (Table 1, Figure 3), whereas no π-π stacking or metallophilic Pt···Pt interactions were observed in the single-crystal X-ray data of **1** [58]. The molecules of the complex in crystals of pure **1** [58] and in the **1**·1/2(1,4-DITFB) adduct differed in the orientation of the aryl rings in the 4-(phenylethynyl)phenyl isocyanide ligand (Figure S1.3, see Supplementary Materials). For **1**·1/2(1,4-DITFB), both aryl rings were nearly coplanar (the dihedral angle between two aryl rings was 4.9(5)°), whereas in pure **1** [58], the angle between both aryl rings was much larger (168(18)°).

The co-crystal exhibited C–I···Cl–Pt short contacts between an I-substituent of 1,4-DITFB and the coordinated chloride of **1**; the C–I···Cl–Pt short contact comprised 86% of the sum of the Bondi vdW radii [86] and the corresponding angle around the I center was close to 180° (C–I···Cl = 174.6(4)°; Table 1). These geometrical parameters led to the determination of this short contact as halogen bonding (abbreviated as HaB). According to the IUPAC criteria for Type II halogen interactions [87], appropriate theoretical calculations are required to prove the HaB character of the bonding (see later). The I atom from 1,4-DITFB acted as the σ-hole donor and interacted with a nucleophilic lump of Cl atom from **1**.

Other infrequent contacts in the crystal structure of **1**·1/2(1,4-DITFB) were N_{CN}···Pt (3.536 Å, Figure 3). For the N_{CN}···Pt separation, the N···Pt distance (3.536(10) Å) was larger than Bondi $\Sigma_{vdW}N$ + Pt 3.27 Å [88] but shorter than the sum of Batsanov $\Sigma_{vdW}N$ + Pt 3.65 Å [88] and Alvarez $\Sigma_{vdW}N$ + Pt 3.95 Å [89]. The N_{CN}···Pt contact exhibited a comparable length to those in the previous structures of cyclometallated Pt^{II}

complexes (Table S1.3, see Supplementary Materials) and even in other (RNC)M species (see CSD search with brief analysis for $N_{CN} \cdots M$ contacts in Ref. [29]). In addition, the second determined key factor was the ungular parameter $\angle(C \equiv N \cdots Pt)$ of this contact. These angles should have occurred near 90°, and a minimal deviation close to 0° was found [29,57]. Based on the XRD data, we observed that the $\angle(C \equiv N \cdots Pt)$ angle with 86.7(4)° satisfied the attributed ungular parameters. The data-based geometry considerations collected in Table 1 indicate that the Pt nucleophilic site directed to the nitrogen of the $C \equiv N$ group. The presence of the π-hole$(CN) \cdots d_z^2(Pt)$ interaction was verified with a theoretical study (see later).
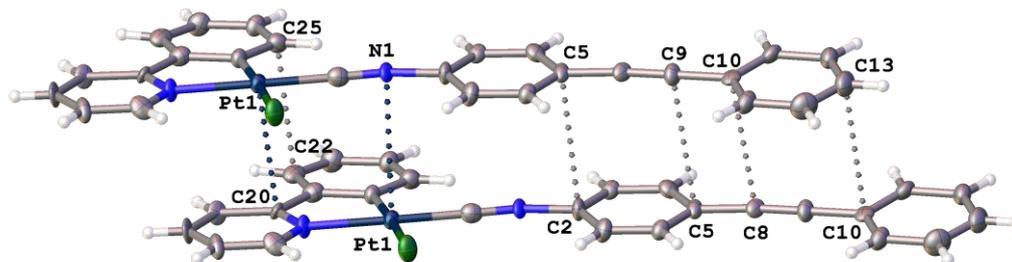
Figure 3. Identified noncovalent contacts in the crystal structure of **1**·1/2(1,4-DITFB). Gray dotted line indicates the π-π stacking, dark blue—the $N_{CN} \cdots Pt$ and $Pt \cdots \pi$ contacts.

The $I \cdots Cl$ HaB, on the one hand, and the combination of $N_{CN} \cdots Pt$ contacts with $\pi \cdots \pi$ interactions, on the other hand, achieved a 2D extended ladder-type architecture (Figure 4). Different 2D ladder arrays of molecules were linked via C–$H \cdots Cl$ (d(C,Cl) 3.66 Å) and C–$H \cdots F$ (d(C,F) 3.38 Å) contacts (Figure S1.2).
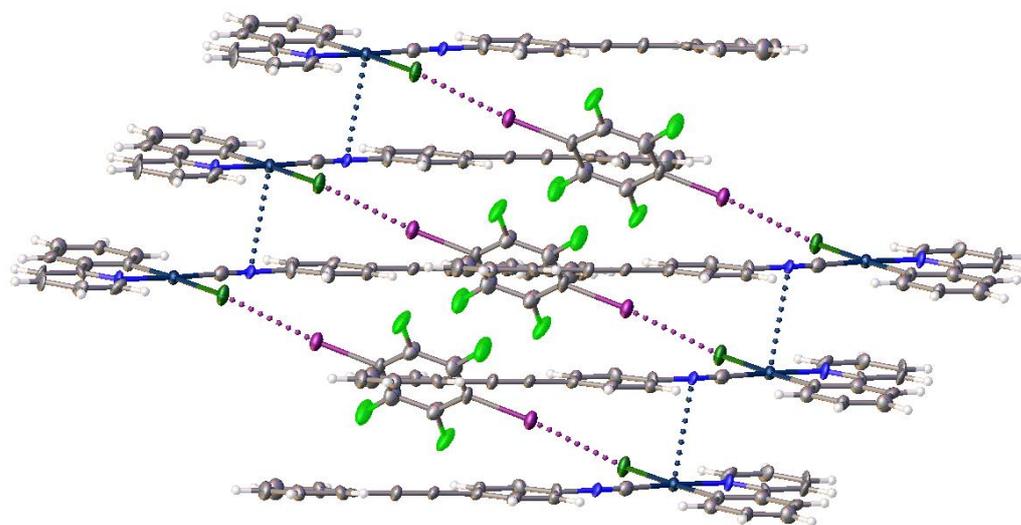
Figure 4. Noncovalent interactions of 2D ladder-type architecture. Purple dotted line indicates the Pt–Cl$\cdots$I–C HaBs, dark blue—the $N_{CN} \cdots Pt$ contact.

Previously [37], complex **1** was co-crystallized with bromo-substituted perfluorinated arenes, namely, bromopentafluorobenzene (IC_6F_5) and 1,2-dibromotetrafluorobenzene (o-$Br_2C_6F_4$); these crystallizations led to a completely different type of co-crystal, namely, 1:1 co-crystals **1**·(BrC_6F_5) and **1**·(1,2-$Br_2C_6F_4$). Similar to **1**·1/2(1,4-DITFB), co-crystals **1**·(BrC_6F_5) and **1**·(1,2-$Br_2C_6F_4$) exhibited C–Br$\cdots$Cl–Pt HaBs, but the packing of **1**·(BrC_6F_5) and **1**·(1,2-$Br_2C_6F_4$) formed alternating layers of organometallics and perfluorinated arenes with weak Br-^{F}Arenes$\cdots$Pt contacts.

Table 1. Geometrical parameters of short contacts in the structure of **1**·1/2(1,4-DITFB).

Contact	Distance, Å	Angle, °	R[a/b/c]
I···Cl	3.204(3)	∠(C–I···Cl) 174.6(4)	0.86/0.82/0.83
N_{CN}···Pt	3.536(10)	∠(C–N···Pt) 86.7(4)°	1.08/0.97/0.90
C25···C22	3.438(19)	∠(C21–C22···C25) 87.7(9)°	1.01/1.01/0.97
Pt1···C20	3.612(13)	∠(C21–C20···Pt) 86.7(4)°	1.06/0.96/0.89
C5···C2	3.462(19)	∠(N1–C2···C5) 83.7(7)°	1.02/1.02/0.98
C9···C5	3.504 (19)	∠(C8–C9···C5) 96.7(9)°	1.03/1.03/0.99
C10···C8	3.487(19)	∠(C9–C8···C10) 96.9(9)°	1.03/1.03/0.99
C13···C10	3.520(2)	∠(C9–C10···C13) 86.4(8)°	1.04/1.04/0.99

R = d(X···Y)/(ΣvdW (X + Y)), X = I, N; Y = Cl, Pt; [a] Bondi [88], [b] Batsanov [88], and [c] Alvarez [89] van der Waals radii were used.

3.2. Theoretical Study

The DFT calculations, MEP analysis [90–92], and the quantum theory of atoms in molecules (QTAIM) [80] with a noncovalent interaction plot (NCI plot) [93,94] and the electron localization function (ELF) [95–97] were used to reveal the nature of I···Cl and N_{CN}···Pt interactions in real space. The discussion detailed in the following subsections is based on the single-point calculations for the XRD geometries of our systems (i.e., without optimization) due to the nature of the crystal-packing effects of the intermolecular interactions in **1**·1/2(1,4-DITFB), whereas within the studies of interactions, the electrostatics played a secondary role.

First, we computed the MEP surfaces to study the electron-rich and electron-poor parts of **1** and 1,4-DITFB (Figure 5). As expected, the MEP minimum of complex **1** was located at the chloride ligand (−39.5 kcal/mol). At the Pt atom, the MEP was also negative (−23.4 kcal/mol), which was determined by mutual contribution of the anionic ligands and the $d_z{}^2$ orbitals at the Pt^{II} site. In the isocyano group, the MEP was also negative (−9.8 at C and −2.1 at N, measured perpendicular to the molecular plane) but less negative than the charge of the Pt atom. At the aromatic H-atoms, the MEP maximum, ranging from 13.4 to 25.2 kcal/mol, was large and positive. The MEP maximum of 1,4- DITFB was located at the iodine σ-hole (31.1 kcal/mol).
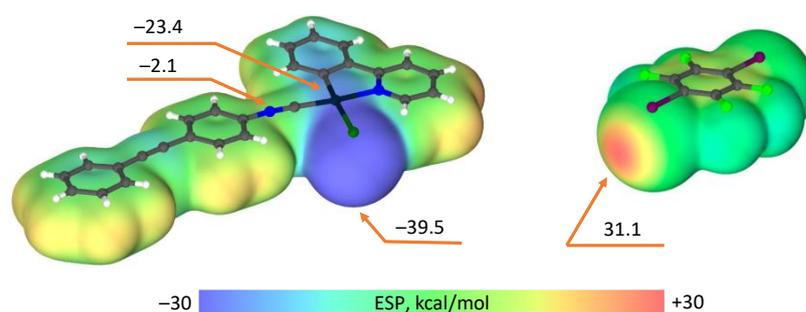
Figure 5. MEP surfaces of **1** (**left**) and 1,4-DITFB (**right**). Energies at selected points are indicated in kcal/mol. Isovalue 0.001 a.u.

For a more comprehensive understanding of the nature of the noncovalent interactions, we employed DFT calculations. These calculations were performed on two different supramolecular associates, namely, (**1**·(1,4-DITFB)) and (**1**)$_2$, denoted as "**A**" and "**B**," respectively, which exemplify the two binding modes shown in Figure 4. The QTAIM/NCI plot analyses are given in Figure 6 as a 3D visualization of various noncovalent interactions and in Figure S2.1 (see Supplementary Materials) as a typical NCI plot, i.e., a scatter graph of RDG vs. sign($λ_2$)ρ, namely, the product of the sign of $λ_2$ (the second largest eigenvalue of the electron density Hessian matrix) and ρ (the electron density). In the supramolecular

associate **A**, the HaB was characterized by a bond critical point (BCP), a bond path, and a disk-shaped reduced density gradient (RDG) isosurface that connects I to Cl atoms. The position of the I atom coincided with the MEP minimum, as shown in Figure 5. We defined energies for this HaB according to the procedures proposed by Espinosa et al. [98], Vener et al. [99], and Tsirelson et al. [100], and it can be stated that the estimated strength was in the range of 3.0–4.6 kcal/mol (Table 2). The I atoms were also connected to the aromatic H atoms' adjacent BCPs and bond paths, revealing the presence of ancillary C−H···I hydrogen bonds. Dimer **B** was connected by seven (3, −1) bond critical points (BCPs, shown as small blue spheres) and bond paths (black lines). One bond BCP connected N and Pt atoms, disclosing the existence of N_{CN}··· Pt interactions. Dimer **B** also had BCPs and bond paths connecting the Pt to a C atom of the aromatic ring, demonstrating the occurrence of Pt···π interactions. The additional five BCPs and bond paths connected the C atoms of the aromatic rings and the alkyl group, corresponding to the π··· π interactions in dimer **B**.

The complexation energy for the supramolecular associate **A** was −8.0 kcal/mol and could be mainly attributed to the HaB, with small participation of the hydrogen bonds, which is supported by the NCI plot analyses. The dimerization energy for dimer **B** was ΔE = −23.5 kcal/mol, which combined the intermolecular interactions of Pt1···N1, Pt1···C20, and π-π stacking. There are reports indicating a significant contribution of stacking interactions between chelate and aromatic rings and π-π stacking for the formation of the supramolecular architecture of metal-containing particles in the solid state [101,102], so it is likely that in the case of **1**·1/2(1,4-DITFB), these interactions also make an undeniable contribution to the organization and stabilization of the final crystal structure. Nevertheless, π-π stacking interactions belong to nondirectional intermolecular interactions, and among all the noncovalent interactions found in dimer **B**, only the Pt···N interaction has a directional character [29,57]. Therefore, and also considering the fact that intermolecular (isocyano group)···Pt^{II} interactions have previously been reconsidered with respect to their influence on photophysical performance [29], the Pt···N interaction was further investigated theoretically. The energy for dimer 1,4-DITFB···1,4-DITFB ((1,4-DITFB)$_2$) was −6.0 kcal/mol, which is weaker than the dimerization energy for supramolecular associates **A** and **B**.
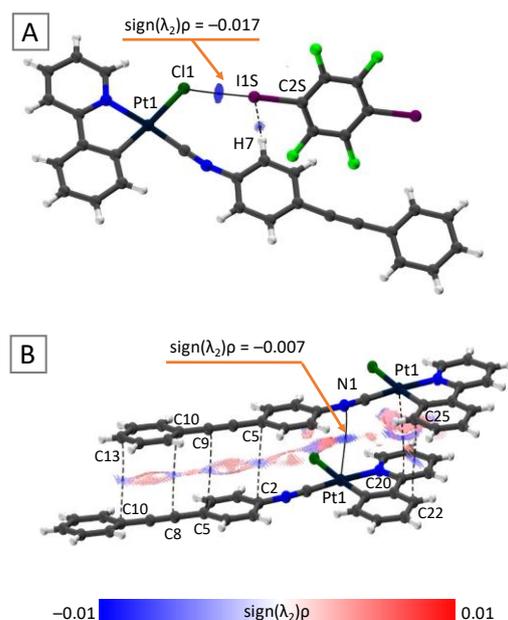
Figure 6. QTAIM and NCI plot analyses of the model supramolecular associates (**A**,**B**). Only intermolecular interactions are represented. Solid line indicates the Pt–Cl···I–C HaBs and N_{CN}··· Pt contact, dashed line indicates the Pt··· π and π··· π contacts.

Table 2. The BSSE-corrected complexation energies ΔE (kcal/mol) for dimers **A** and **B** (Figure 6a,b) and BCP topological analysis for I···Cl and N_{CN}···Pt interactions, where $sign(\lambda 2)\rho(r)$ is the electron density, $\nabla^2\rho(r)$ is the Laplacian of the electron density, $G(r)$ is the electronic kinetic energy density, $V(r)$ is the electronic potential energy density, and $H(r)$ is the local electronic energy density.

Supramolecular Associate	Contact	Sign(λ^2)$\rho(r)$	$\nabla^2\rho(r)$	$G(r)$	$V(r)$	$H(r)$	WBI	E_{int}[a/b/c/d]	ΔE, kcal/mol
A	I1S···Cl1	−0.017	0.0481	0.011	−0.010	0.001	0.07	4.3/4.6/3.1/3.0	−8.0
	I1S···H7	−0.005	0.0123	0.002	−0.002	0.001	0.002	−/−/0.6/0.7	
B	Pt1···N1	−0.007	0.0229	0.005	−0.004	0.001	0.002	−	−23.5
	C25···C22	−0.005	0.0144	0.003	−0.002	0.001	0.002	−	
	Pt1···C20	−0.007	0.0193	0.004	−0.003	0.001	0.002	−	
	C5···C2	−0.004	0.0149	0.003	−0.002	0.001	0.001	−	
	C9···C5	−0.004	0.0144	0.003	−0.002	0.001	0.001	−	
	C10···C8	−0.004	0.0146	0.003	−0.002	0.001	0.001	−	
	C13···C10	−0.004	0.0137	0.003	−0.002	0.001	0.001	−	

[a] $E_{int} = 0.68(−V(r))$ (Tsirelson's empirical correlation between the interaction energy and potential energy density of electrons at the bond critical points (3, −1) for noncovalent interactions I···X [100]). [b] $E_{int} = 0.67G(r)$ (Tsirelson's empirical correlation between the interaction energy and kinetic energy density of electrons at the bond critical points (3, −1) for noncovalent interactions I···X [100]). [c] $E = −V(r)/2$ (Espinosa's empirical correlation for the estimation of the energies of the hydrogen bonds [98]). [d] $E = 0.429G(r)$ (Vener's empirical correlation for the estimation of the energies of the hydrogen bonds [99]).

Analysis of ELF and electron density/electrostatic potential distribution along the bond path. To determine the philicities of noncovalently interacting atoms, we used ELF projections with critical points and bond paths from QTAIM electron density topology. In the ELF projection for the I···Cl bond, the path went through the lone-pair orange area of Cl and the blueish area with low ELF values around I, which confirmed the σ-hole of the I atom and the HaB nature of the noncovalent interaction (Figure 7, left) [52,103–106] with the nucleophilic chloride ligand and the electrophilic I centers of 1,4-DITFB.

The Pt···N bond path between the metal center and the N atom passed through the filled $d_z{}^2$ orbitals of the Pt atom with small values of ELF, indicating the weakly nucleophilic manner of the metal atom in the weakly polar N_{CN}···Pt interaction (Figure 7, right).
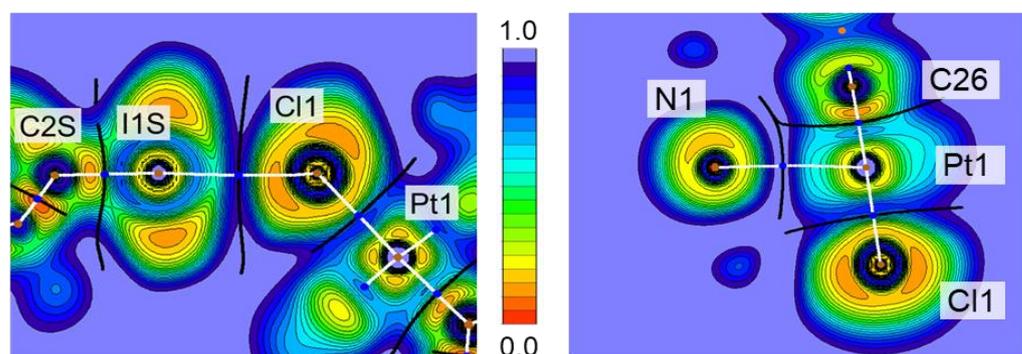
Figure 7. ELF projections (contour lines with 0.05 step), bond paths (white lines), zero-flux surface projections (black lines), bond CPs (blue dots), nuclear CPs (brown dots), and ring CPs (orange dots) for the I···Cl HaBs (**left**) and π-hole(CN)···$d_z{}^2$(Pt) interaction (**right**).

The comparison of the minima of the electron density (ED) and the electrostatic potential (ESP) along the binding path also allowed us to verify the affinities, since, in the case of a polar noncovalent interaction, the ESP minimum shifts towards the nucleophilic atom and the ED minimum shifts towards the electrophilic site [107]. The analysis of the 1D profiles of the ED and ESP functions [108] along the I···Cl bond path showed the

clear nucleophilic nature of the Cl atom with the shift in the ESP minimum toward it, whereas the ED minimum shifted toward the electrophilic I atom, which also confirmed the HaB nature of these noncovalent C–I···Cl–Pt interactions (Figure 8, Left). At the same time, for the N_{CN}··· Pt interaction, the ED and ESP minima almost overlapped with the feeble Pt-directed ESD and C-directed ED minima shifts, meaning that the N_{CN}··· Pt interaction should be regarded as a π-hole(CN)···d_z^2(Pt) interaction, with the N atom as an electrophile and the Pt center as a nucleophile (Figure 8, Right).
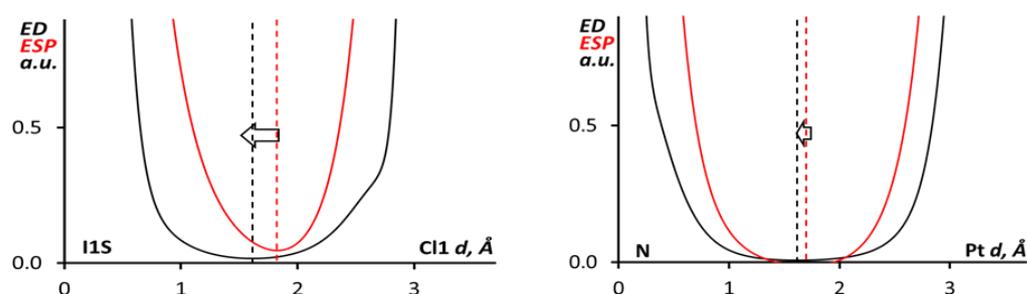
Figure 8. The ED (black) vs. ESP (red) minima along the bond paths for the I···Cl HaBs (**left**) and π-hole(CN)···d_z^2(Pt) interaction (**right**).

3.3. Photophysical Measurements

The photophysical properties of **1**·1/2(1,4-DITFB) co-crystals were studied in the solid state and were compared with the photophysical properties of **1**, which were previously described [37]. Similarity to **1**, the luminescence spectra of **1**·1/2(1,4-DITFB) (Figure 9) were broad, partially structured, and, in accordance with the literature data, could be assigned to a metal-perturbed ^{3}LC intraligand transition with a small admixture of ^{3}MLCT [37]. The difference between **1** and **1**·1/2(1,4-DITFB) is that the adduct showed an additional longer-wavelength emission band in the 550–750 nm region. These findings can be interpreted in terms of the formation of bi-molecular states such as ground-state dimers and/or excited states—excimers [109]. Monoexponential transient decays were observed for the emission at 517 nm and at 617 nm. The lifetimes obtained from exponential decay fits were characterized by τ_{obs} = 0.03 μs in both cases. In addition, the co-crystallization of **1** with 1,4-DITFB provided to increase the Φ_{em} up to 0.02%, whereas the **1** was extremely weakly emissive at RT. These data are coherent with our DFT computational data indicating a significant dimerization energy for supramolecular associates, which is likely to have affected the increase in molecular rigidity. Therefore, our results and other examples of adducts of cyclometallated platinum complexes with perfluoroarenes or haloperfluoroarenes shown in Figure 1 indicate that, in all cases, the formation of adducts led to an increase in the quantum yield of phosphorescence, with insignificant spectral changes.
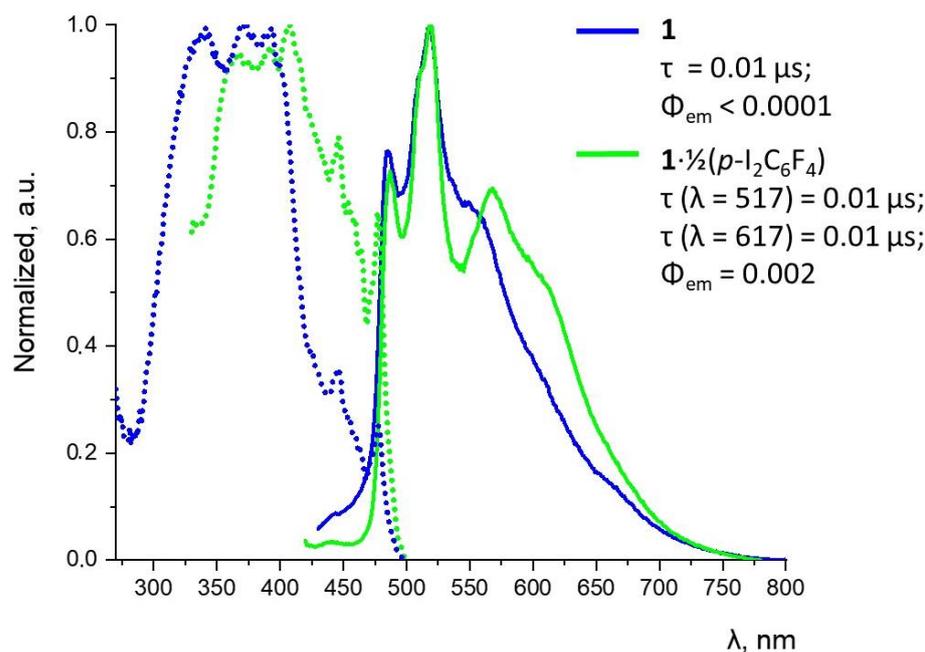
Figure 9. Normalized solid-state excitation and emission spectra for **1** (λ_{ex} = 410 nm) and **1**·1/2(1,4-DITFB) (λ_{ex} = 405 nm) (298 K).

4. Conclusions

The co-crystallization of the Pt^{II} isocyanide complex [Pt(ppy)Cl(CNC$_6$H$_4$-C≡C–Ph)] (**1**) with 1,4-diiodotetrafluorobenzene (1,4-DITFB) yielded **1**·1/2(1,4-DITFB) adduct. During the inspection of the X-ray structure of **1**·1/2(1,4-DITFB), the presence of several attractive contacts was observed. The first one was C–I···Cl–Pt short contacts, for which the I substituent of 1,4-DITFB interacted with the coordinated chloride and whose geometrical parameters were comparable to I···Cl halogen bonding. The second one was the combined π-hole(isocyano group)··· d_z^2[Pt^{II}], and stacking interactions between chelate and aromatic rings and π-π stacking led to the formation of the supramolecular architecture of metal-containing particles in the solid state. Examination of the photophysical properties revealed that the formation of the adduct led to an increase in the quantum yield of the phosphorescence, with insignificant spectral changes.

Supplementary Materials: The following supporting information can be downloaded at: https://www.mdpi.com/article/10.3390/inorganics11100403/s1, Figure S1.1: Molecular view of **1**·1/2(1,4-DITFB). Thermal ellipsoids for are drawn at the 50% probability level; Figure S1.2: A fragment of the crystal packing of **1**·1/2(1,4-DITFB); Figure S1.3: Molecule structures of complex **1** in the crystals of pure **1** [58] and adduct **1**·1/2(1,4-DITFB); Figure S1.4: The measured powder X-ray diffraction patterns of crystalline **1**·1/2(1,4-DITFB); Figure S2.1: RDG(r)–sign[$\lambda 2(\mathbf{r})$]$\rho(\mathbf{r})$ plot for the I···Cl HaB in (left) and NCN···Pt contact (right) in the crystal structure of **1**·1/2(1,4-DITFB); Figure S2.2: Left: ELF projections (contour lines with 0.05 step), bond paths (white lines), zero-flux surface projections (black lines), bond CPs (blue dots), nuclear CPs (brown dots), and ring CPs (orange dots). Right: The ED (black) vs. ESP (red) minima along the bond paths for the I···Cl HaB in the crystal structure of **1**·1/2(1,4-DITFB); Figure S2.3: Left: ELF projections (contour lines with 0.05 step), bond paths (white lines), zero-flux surface projections (black lines), bond CPs (blue dots), nuclear CPs (brown dots), and ring CPs (orange dots). Right: The ED (black) vs. ESP (red) minima along the bond paths for the NCN···Pt contact in the crystal structure of **1**·1/2(1,4-DITFB); Table S1.1: Crystal data and structure refinement for **1**·1/2(1,4-DITFB) adduct; Table S1.2: Selected bond lengths (Å) and angles (°) for **1**·1/2(1,4-DITFB); Table S1.3: CSD data analysis. References [29,43,49,110–112] are cited in the Supplementary Materials.

Author Contributions: Conceptualization, S.A.K., D.M.I. and M.A.K.; methodology, E.V.A., A.M.C. and S.A.K.; investigation, E.V.A., A.M.C. and S.A.K.; writing—original draft preparation, E.V.A., S.A.K. and D.M.I.; writing—review and editing, E.V.A., S.A.K., D.M.I. and M.A.K.; visualization, E.V.A., A.M.C., S.A.K., D.M.I. and M.A.K.; supervision, M.A.K. and D.M.I.; project administration, S.A.K. and M.A.K. All authors have read and agreed to the published version of the manuscript.

Data Availability Statement: The data that support the findings of this study are available upon reasonable request from the authors.

Conflicts of Interest: The authors declare no conflict of interest.

References

1. Tang, M.C.; Chan, A.K.W.; Chan, M.Y.; Yam, V.W.W. Platinum and Gold Complexes for OLEDs. *Top. Curr. Chem.* **2016**, *374*, 46. [CrossRef] [PubMed]
2. Zhuang, Y.L.; Guo, S.; Deng, Y.J.; Liu, S.J.; Zhao, Q. Electroluminochromic Materials and Devices Based on Metal Complexes. *Chem. Asian J.* **2019**, *14*, 3791–3802. [CrossRef] [PubMed]
3. Zhang, Q.-C.; Xiao, H.; Zhang, X.; Xu, L.-J.; Chen, Z.-N. Luminescent oligonuclear metal complexes and the use in organic light-emitting diodes. *Chem. Soc. Rev.* **2019**, *378*, 121–133. [CrossRef]
4. Ibrahim-Ouali, M.; Dumur, F. Recent Advances on Metal-Based Near-Infrared and Infrared Emitting OLEDs. *Molecules* **2019**, *24*, 1412. [CrossRef] [PubMed]
5. Mahoro, G.U.; Fernandez-Cestau, J.; Renaud, J.-L.; Coto, P.B.; Costa, R.D.; Gaillard, S. Recent Advances in Solid-State Lighting Devices Using Transition Metal Complexes Exhibiting Thermally Activated Delayed Fluorescent Emission Mechanism. *Adv. Opt. Mater.* **2020**, *8*, 2000260. [CrossRef]
6. Lee, S.; Han, W.-S. Cyclometalated Ir(III) complexes towards blue-emissive dopant for organic light-emitting diodes: Fundamentals of photophysics and designing strategies. *Inorg. Chem. Front.* **2020**, *7*, 2396. [CrossRef]
7. Li, X.; Xie, Y.; Li, Z. Diversity of Luminescent Metal Complexes in OLEDs: Beyond Traditional Precious Metals. *Chem. Asian J.* **2021**, *16*, 2817–2829. [CrossRef] [PubMed]
8. Zhou, X.; Lee, S.; Xu, Z.; Yoon, J. Recent Progress on the Development of Chemosensors for Gases. *Chem. Rev.* **2015**, *115*, 7944–8000. [CrossRef]
9. Abd Elhameid, M.K.; Ryad, N.; My, A.-S.; Mohammed, M.R.; Ismail, M.M.; El Meligie, S. Design, Synthesis and Screening of 4,6-Diaryl Pyridine and Pyrimidine Derivatives as Potential Cytotoxic Molecules. *Chem. Pharm. Bull.* **2018**, *66*, 939–952. [CrossRef]
10. Ma, D.-L.; Wong, S.-Y.; Kang, T.-S.; Ng, H.-P.; Han, Q.-B.; Leung, C.-H. Iridium(III)-based chemosensors for the detection of metal ions. *Methods* **2019**, *168*, 3–17. [CrossRef]
11. Prier, C.K.; Rankic, D.A.; MacMillan, D.W. Visible light photoredox catalysis with transition metal complexes: Applications in organic synthesis. *Chem. Rev.* **2013**, *113*, 5322–5363. [CrossRef]
12. Arias-Rotondo, D.M.; McCusker, J.K. The photophysics of photoredox catalysis: A roadmap for catalyst design. *Chem. Soc. Rev.* **2016**, *45*, 5803–5820. [CrossRef] [PubMed]
13. Glaser, F.; Wenger, O.S. Recent progress in the development of transition-metal based photoredox catalysts. *Coord. Chem. Rev.* **2020**, *405*, 213129. [CrossRef]
14. Chan, A.Y.; Perry, I.B.; Bissonnette, N.B.; Buksh, B.F.; Edwards, G.A.; Frye, L.I.; Garry, O.L.; Lavagnino, M.N.; Li, B.X.; Liang, Y.; et al. Metallaphotoredox: The Merger of Photoredox and Transition Metal Catalysis. *Chem. Rev.* **2021**, *122*, 1485–1542. [CrossRef] [PubMed]
15. Chi, Y.; Chou, P.T. Transition-metal phosphors with cyclometalating ligands: Fundamentals and applications. *Chem. Soc. Rev.* **2010**, *39*, 638–655. [CrossRef] [PubMed]
16. Haque, A.; Xu, L.; Al-Balushi, R.A.; Al-Suti, M.K.; Ilmi, R.; Guo, Z.; Khan, M.S.; Wong, W.-Y.; Raithby, P.R. Cyclometallated tridentate platinum(ii) arylacetylide complexes: Old wine in new bottles. *Chem. Soc. Rev.* **2019**, *48*, 5547–5563. [CrossRef] [PubMed]
17. To, W.P.; Wan, Q.Y.; Tong, G.S.M.; Che, C.M. Recent Advances in Metal Triplet Emitters with d(6), d(8), and d(10) Electronic Configurations. *Trends Chem.* **2020**, *2*, 796–812. [CrossRef]
18. Yam, V.W.W.; Law, A.S.Y. Luminescent d(8) metal complexes of platinum(II) and gold(III): From photophysics to photofunctional materials and probes. *Coord. Chem. Rev.* **2020**, *414*, 213298. [CrossRef]

19. Li, K.; Chen, Y.; Wang, J.; Yang, C. Diverse emission properties of transition metal complexes beyond exclusive single phosphorescence and their wide applications. *Coord. Chem. Rev.* **2021**, *433*, 213755. [CrossRef]
20. Sutton, G.D.; Olumba, M.E.; Nguyen, Y.H.; Teets, T.S. The diverse functions of isocyanides in phosphorescent metal complexes. *Dalton Trans.* **2021**, *50*, 17851. [CrossRef]
21. Jain, V.K. Cyclometalated group-16 compounds of palladium and platinum: Challenges and opportunities. *Coord. Chem. Rev.* **2021**, *427*, 213546. [CrossRef]
22. Cruz-Cabeza, A.J.; Reutzel-Edens, S.M.; Bernstein, J. Facts and fictions about polymorphism. *Chem. Soc. Rev.* **2015**, *44*, 8619–8635. [CrossRef] [PubMed]
23. Wang, C.; Li, Z. Molecular conformation and packing: Their critical roles in the emission performance of mechanochromic fluorescence materials. *Mater. Chem. Front.* **2017**, *1*, 2174–2194. [CrossRef]
24. Lu, B.; Liu, S.; Yan, D. Recent advances in photofunctional polymorphs of molecular materials. *Chin. Chem. Lett.* **2019**, *30*, 1908–1922. [CrossRef]
25. Ohno, K.; Hasebe, M.; Nagasawa, A.; Fujihara, T. Change in Luminescence Induced by Solution-Mediated Phase-Transition of Cyclometalated Platinum(II) Complex with Isoquinoline Carboxylate. *Inorg. Chem.* **2017**, *56*, 12158–12168. [CrossRef]
26. Norton, A.E.; Abdolmaleki, M.K.; Liang, J.M.; Sharma, M.; Golsby, R.; Zoller, A.; Krause, J.A.; Connick, W.B.; Chatterjee, S. Phase transformation induced mechanochromism in a platinum salt: A tale of two polymorphs. *Chem. Comm.* **2020**, *56*, 10175–10178. [CrossRef] [PubMed]
27. Han, Y.; Gao, Z.; Wang, C.; Zhong, R.; Wang, F. Recent progress on supramolecular assembly of organoplatinum(II) complexes into long-range ordered nanostructures. *Coord. Chem. Rev.* **2020**, *414*, 213300. [CrossRef]
28. Kimura, M.; Yoshida, M.; Fujii, S.; Miura, A.; Ueno, K.; Shigeta, Y.; Kobayashi, A.; Kato, M. Liquid–liquid interface-promoted formation of a porous molecular crystal based on a luminescent platinum(ii) complex. *Chem. Commun.* **2020**, *56*, 12989–12992. [CrossRef]
29. Katkova, S.A.; Mikherdov, A.S.; Sokolova, E.V.; Novikov, A.S.; Starova, G.L.; Kinzhalov, M.A. Intermolecular (Isocyano group)···PtII interactions involving coordinated isocyanides in cyclometalated PtII complexes. *J. Mol. Struct.* **2022**, *1253*, 132230. [CrossRef]
30. Aliprandi, A.; Genovese, D.; Mauro, M.; Cola, L.D. Recent Advances in Phosphorescent Pt(II) Complexes Featuring Metallophilic Interactions: Properties and Applications. *Chem. Lett.* **2015**, *44*, 1152–1169. [CrossRef]
31. Tiekink, E.R.T. Supramolecular assembly based on "emerging" intermolecular interactions of particular interest to coordination chemists. *Coord. Chem. Rev.* **2017**, *345*, 209–228. [CrossRef]
32. Gray, H.B.; Záliš, S.; Vlček, A. Electronic structures and photophysics of d8-d8 complexes. *Coord. Chem. Rev.* **2017**, *345*, 297–317. [CrossRef]
33. Ravotto, L.; Ceroni, P. Aggregation induced phosphorescence of metal complexes: From principles to applications. *Coord. Chem. Rev.* **2017**, *346*, 62–76. [CrossRef]
34. Yoshida, M.; Kato, M. Regulation of metal–metal interactions and chromic phenomena of multi-decker platinum complexes having π-systems. *Coord. Chem. Rev.* **2018**, *355*, 101–115. [CrossRef]
35. Sivchik, V.V.; Solomatina, A.I.; Chen, Y.-T.; Karttunen, A.J.; Tunik, S.P.; Chou, P.-T.; Koshevoy, I.O. Halogen Bonding to Amplify Luminescence: A Case Study Using a Platinum Cyclometalated Complex. *Angew. Chem. Int. Ed.* **2015**, *54*, 14057–14060. [CrossRef] [PubMed]
36. Sivchik, V.; Sarker, R.K.; Liu, Z.Y.; Chung, K.Y.; Grachova, E.V.; Karttunen, A.J.; Chou, P.T.; Koshevoy, I.O. Improvement of the Photophysical Performance of Platinum-Cyclometalated Complexes in Halogen-Bonded Adducts. *Chem. Eur. J.* **2018**, *24*, 11475–11484. [CrossRef] [PubMed]
37. Katkova, S.A.; Luzyanin, K.V.; Novikov, A.S.; Kinzhalov, M.A. Modulation of luminescence properties for [cyclometalated]-PtII(isocyanide) complexes upon co-crystallisation with halosubstituted perfluorinated arenes. *New J. Chem.* **2021**, *45*, 2948–2952. [CrossRef]
38. Koshevoy, I.O.; Krause, M.; Klein, A. Non-covalent intramolecular interactions through ligand-design promoting efficient photoluminescence from transition metal complexes. *Coord. Chem. Rev.* **2020**, *405*, 213094. [CrossRef]
39. Wang, W.; Zhang, Y.; Jin, W.J. Halogen bonding in room-temperature phosphorescent materials. *Coord. Chem. Rev.* **2020**, *404*, 213107. [CrossRef]
40. Yan, D.; Evans, D.G. Molecular crystalline materials with tunable luminescent properties: From polymorphs to multi-component solids. *Mater. Horiz.* **2014**, *1*, 46–57. [CrossRef]
41. Rozhkov, A.V.; Ananyev, I.V.; Gomila, R.M.; Frontera, A.; Kukushkin, V.Y. π-Hole·dz2[PtII] Interactions with Electron-Deficient Arenes Enhance the Phosphorescence of PtII-Based Luminophores. *Inorg. Chem.* **2020**, *59*, 9308–9314. [CrossRef]
42. Samandar Sangari, M.; Golbon Haghighi, M.; Nabavizadeh, S.M.; Pfitzner, A.; Rashidi, M. Influence of ancillary ligands on the photophysical properties of cyclometalated organoplatinum(ii) complexes. *New J. Chem.* **2018**, *42*, 8661–8671. [CrossRef]
43. Martínez-Junquera, M.; Lara, R.; Lalinde, E.; Moreno, M.T. Isomerism, aggregation-induced emission and mechanochromism of isocyanide cycloplatinated(ii) complexes. *J. Mater. Chem. C* **2020**, *8*, 7221–7233. [CrossRef]
44. Martinez-Junquera, M.; Lalinde, E.; Moreno, M.T.; Alfaro-Arnedo, E.; Lopez, I.P.; Larrayoz, I.M.; Pichel, J.G. Luminescent cyclometalated platinum(ii) complexes with acyclic diaminocarbene ligands: Structural, photophysical and biological properties. *Dalton Trans.* **2021**, *50*, 4539–4554. [CrossRef]

45. Horiuchi, S.; Umakoshi, K. Recent advances in pyrazolato-bridged homo- and heterometallic polynuclear platinum and palladium complexes. *Coord. Chem. Rev.* **2023**, *476*, 214924. [CrossRef]

46. Amouri, H. Luminescent Complexes of Platinum, Iridium, and Coinage Metals Containing N-Heterocyclic Carbene Ligands: Design, Structural Diversity, and Photophysical Properties. *Chem. Rev.* **2023**, *123*, 230–270. [CrossRef] [PubMed]

47. Kinzhalov, M.A.; Grachova, E.V.; Luzyanin, K.V. Tuning the Luminescence of Transition Metal Complexes with Acyclic Diaminocarbene Ligands. *Inorg. Chem. Front.* **2022**, *9*, 417. [CrossRef]

48. Paziresh, S.; Babadi Aghakhanpour, R.; Fuertes, S.; Sicilia, V.; Niroomand Hosseini, F.; Nabavizadeh, S.M. A double rollover cycloplatinated(II) skeleton: A versatile platform for tuning emission by chelating and non-chelating ancillary ligand systems. *Dalton Trans.* **2019**, *48*, 5713. [CrossRef]

49. Fornies, J.; Sicilia, V.; Borja, P.; Casas, J.M.; Diez, A.; Lalinde, E.; Larraz, C.; Martin, A.; Moreno, M.T. Luminescent Benzoquinolate-Isocyanide Platinum(II) Complexes: Effect of Pt···Pt and π···π Interactions on their Photophysical Properties. *Chem. Asian J.* **2012**, *7*, 2813–2823. [CrossRef]

50. Sicilia, V.; Arnal, L.; Escudero, D.; Fuertes, S.; Martin, A. Chameleonic Photo- and Mechanoluminescence in Pyrazolate-Bridged NHC Cyclometalated Platinum Complexes. *Inorg. Chem.* **2021**, *60*, 12274–12284. [CrossRef]

51. Dobrynin, M.V.; Sokolova, E.V.; Kinzhalov, M.A.; Smirnov, A.S.; Starova, G.L.; Kukushkin, V.Y.; Islamova, R.M. Cyclometalated Platinum(II) Complexes Simultaneously Catalyze the Cross-Linking of Polysiloxanes and Function as Luminophores. *ACS Appl. Polym. Mater.* **2021**, *3*, 857. [CrossRef]

52. Sokolova, E.V.; Kinzhalov, M.A.; Smirnov, A.S.; Cheranyova, A.M.; Ivanov, D.M.; Kukushkin, V.Y.; Bokach, N.A. Polymorph-Dependent Phosphorescence of Cyclometalated Platinum(II) Complexes and Its Relation to Non-covalent Interactions. *ACS Omega* **2022**, *7*, 34454–34462. [CrossRef] [PubMed]

53. Katkova, S.A.; Kozina, D.O.; Kisel, K.S.; Sandzhieva, M.A.; Tarvanen, D.A.; Makarov, S.V.; Porsev, V.V.; Tunik, S.P.; Kinzhalov, M.A. Cyclometalated platinum(II) complexes with acyclic diaminocarbene ligands for OLED application. *Dalton Trans.* **2023**, *52*, 4595–4605. [CrossRef] [PubMed]

54. Eremina, A.A.; Kinzhalov, M.A.; Katlenok, E.A.; Smirnov, A.S.; Andrusenko, E.V.; Pidko, E.A.; Suslonov, V.V.; Luzyanin, K.V. Phosphorescent Iridium(III) Complexes with Acyclic Diaminocarbene Ligands as Chemosensors for Mercury. *Inorg. Chem.* **2020**, *59*, 2209–2222. [CrossRef] [PubMed]

55. Mikherdov, A.S.; Kinzhalov, M.A.; Novikov, A.S.; Boyarskiy, V.P.; Boyarskaya, I.A.; Avdontceva, M.S.; Kukushkin, V.Y. Ligation-Enhanced π-Hole·π Interactions Involving Isocyanides: Effect of π-Hole·π Noncovalent Bonding on Conformational Stabilization of Acyclic Diaminocarbene Ligands. *Inorg. Chem.* **2018**, *57*, 6722–6733. [CrossRef] [PubMed]

56. Kinzhalov, M.A.; Kashina, M.V.; Mikherdov, A.S.; Mozheeva, E.A.; Novikov, A.S.; Smirnov, A.S.; Ivanov, D.M.; Kryukova, M.A.; Ivanov, A.Y.; Smirnov, S.N.; et al. Dramatically Enhanced Solubility of Halide-Containing Organometallic Species in Diiodomethane: The Role of Solvent Complex Halogen Bonding. *Angew. Chem. Int. Ed.* **2018**, *57*, 12785–12789. [CrossRef] [PubMed]

57. Katkova, S.A.; Mikherdov, A.S.; Kinzhalov, M.A.; Novikov, A.S.; Zolotarev, A.A.; Boyarskiy, V.P.; Kukushkin, V.Y. (Isocyano Group π-Hole) dz2-M-II Interactions of (Isocyanide) M-II Complexes, in which Positively Charged Metal Centers (d8-M=Pt, Pd) Act as Nucleophiles. *Chem. Eur. J.* **2019**, *25*, 8590–8598. [CrossRef] [PubMed]

58. Kinzhalov, M.A.; Ivanov, D.M.; Melekhova, A.A.; Bokach, N.A.; Gomila, R.M.; Frontera, A.; Kukushkin, V.Y. Chameleonic metal-bound isocyanides: A π-donating CuI-center imparts nucleophilicity to the isocyanide carbon toward halogen bonding. *Inorg. Chem. Front.* **2022**, *9*, 1655–1665. [CrossRef]

59. Kinzhalov, M.A.; Katkova, S.A.; Doronina, E.P.; Novikov, A.S.; Eliseev, I.I.; Ilichev, V.A.; Kukinov, A.A.; Starova, G.L.; Bokach, N.A. Red photo- and electroluminescent half-lantern cyclometalated dinuclear platinum(II) complex. *Z. Kristallogr. Cryst. Mater.* **2018**, *233*, 795–802. [CrossRef]

60. Katkova, S.A.; Leshchev, A.A.; Mikherdov, A.S.; Kinzhalov, M.A. Synthesis of Cyclometalated Platinum(II) Complex with an Alkynyl-Substituted Isocyanide Ligand, Its Structure and Photophysical Properties. *Russ. J. Gen. Chem.* **2020**, *90*, 648–654. [CrossRef]

61. Sheldrick, G. SHELXT—Integrated space-group and crystal-structure determination. *Acta Cryst. Sect. A* **2015**, *71*, 3–8. [CrossRef] [PubMed]

62. Sheldrick, G. *SADABS-2008/1-Bruker AXS Area Detector Scaling and Absorption Correction*; Bruker AXS: Madison, WI, USA, 2008.

63. Dolomanov, O.V.; Bourhis, L.J.; Gildea, R.J.; Howard, J.A.; Puschmann, H. OLEX2: A complete structure solution, refinement and analysis program. *J. Appl. Crystallogr.* **2009**, *42*, 339–341. [CrossRef]

64. Hohenberg, P.; Kohn, W. Inhomogeneous Electron Gas. *Phys. Rev.* **1964**, *136*, B864–B871. [CrossRef]

65. Kohn, W.; Sham, L.J. Self-Consistent Equations Including Exchange and Correlation Effects. *Phys. Rev.* **1965**, *140*, A1133–A1138. [CrossRef]

66. Parr, R.G.; Weitao, Y. *Density-Functional Theory of Atoms and Molecules*; Oxford University Press: New York, NY, USA, 1995; p. 343.

67. Perdew, J.P.; Burke, K.; Ernzerhof, M. Generalized Gradient Approximation Made Simple. *Phys. Rev. Lett.* **1996**, *77*, 3865–3868. [CrossRef] [PubMed]

68. Grimme, S.; Ehrlich, S.; Goerigk, L. Effect of the damping function in dispersion corrected density functional theory. *J. Comput. Chem.* **2011**, *32*, 1456–1465. [CrossRef] [PubMed]

69. Grimme, S.; Antony, J.; Ehrlich, S.; Krieg, H. A consistent and accurate ab initio parametrization of density functional dispersion correction (DFT-D) for the 94 elements H-Pu. *J. Chem. Phys.* **2010**, *132*, 154104. [CrossRef]

70. Weigend, F.; Ahlrichs, R. Balanced basis sets of split valence, triple zeta valence and quadruple zeta valence quality for H to Rn: Design and assessment of accuracy. *Phys. Chem. Chem. Phys.* **2005**, *7*, 3297–3305. [CrossRef]

71. Weigend, F. Accurate Coulomb-fitting basis sets for H to Rn. *Phys. Chem. Chem. Phys.* **2006**, *8*, 1057–1065. [CrossRef]

72. Frisch, M.J.; Trucks, G.; Schlegel, H.B.; Scuseria, G.E.; Robb, M.A.; Cheeseman, J.; Scalmani, G.; Barone, V.; Mennucci, B.; Petersson, G.A.; et al. *Gaussian 09 Revision A.1*; Gaussian Inc.: Wallingford, CT, USA, 2009.

73. Lu, T.; Chen, F. Multiwfn: A multifunctional wavefunction analyzer. *J. Comput. Chem.* **2012**, *33*, 580–592. [CrossRef]

74. Zhang, J.; Lu, T. Efficient evaluation of electrostatic potential with computerized optimized code. *Phys. Chem. Chem. Phys.* **2021**, *23*, 20323–20328. [CrossRef]

75. Johnson, E.R.; Keinan, S.; Mori-Sanchez, P.; Contreras-Garcia, J.; Cohen, A.J.; Yang, W. Revealing noncovalent interactions. *J. Am. Chem. Soc.* **2010**, *132*, 6498–6506. [CrossRef] [PubMed]

76. Humphrey, W.; Dalke, A.; Schulten, K. VMD: Visual molecular dynamics. *J. Mol. Graph.* **1996**, *14*, 33–38. [CrossRef] [PubMed]

77. Kashina, M.V.; Ivanov, D.M.; Kinzhalov, M.A. The Isocyanide Complexes cis-[MCl2(CNC6H4-4-X)2] (M = Pd, Pt; X = Cl, Br) as Tectons in Crystal Engineering Involving Halogen Bonds. *Crystals* **2021**, *11*, 799. [CrossRef]

78. Bader, R.F.W.; Nguyen-Dang, T.T. Quantum Theory of Atoms in Molecules–Dalton Revisited. In *Advances in Quantum Chemistry*; Löwdin, P.-O., Ed.; Academic Press: Cambridge, MA, USA, 1981; Volume 14, pp. 63–124.

79. Bader, R.F.W.; Bader, R.F. *Atoms in Molecules: A Quantum Theory*; Clarendon Press: Oxford, UK, 1990.

80. Bader, R.F.W. A quantum theory of molecular structure and its applications. *Chem. Rev.* **1991**, *91*, 893–928. [CrossRef]

81. Espinosa, E.; Alkorta, I.; Elguero, J.; Molins, E. From weak to strong interactions: A comprehensive analysis of the topological and energetic properties of the electron density distribution involving X–H F–Y systems. *J. Chem. Phys.* **2002**, *117*, 5529–5542. [CrossRef]

82. Bartashevich, E.V.; Matveychuk, Y.V.; Troitskaya, E.A.; Tsirelson, V.G. Characterizing the multiple non-covalent interactions in N, S-heterocycles–diiodine complexes with focus on halogen bonding. *Comput. Theor. Chem.* **2014**, *1037*, 53–62. [CrossRef]

83. Lamberts, K.; Handels, P.; Englert, U.; Aubert, E.; Espinosa, E. Stabilization of polyiodide chains via anion··· anion interactions: Experiment and theory. *CrystEngComm* **2016**, *18*, 3832–3841. [CrossRef]

84. Zhurko, G.A. Chemcraft 1.8—Graphical Software for Visualization of Quantum Chemistry Computations; Ivanovo, Russia. 2005. Available online: https://scholar.google.com/scholar_lookup?hl=en&publication_year=2004&author=G.+A.+Zhurko&author=D.+A.+Zhurko&title=Chemcraft+-+Graphical+Program+for+Visualization+of+Quantum+Chemistry+Computations (accessed on 29 August 2023).

85. Katkova, S.A.; Eliseev, I.I.; Mikherdov, A.S.; Sokolova, E.V.; Starova, G.L.; Kinzhalov, M.A. Cyclometalated Platinum(II) Complexes with Nitrile and Isocyanide Ligands: Synthesis, Structure, and Photophysical Properties. *Russ. J. Gen. Chem.* **2021**, *91*, 393. [CrossRef]

86. Bondi, A. Van der Waals Volumes and Radii. *J. Phys. Chem.* **1964**, *68*, 441–451. [CrossRef]

87. Desiraju, G.R.; Ho, P.S.; Kloo, L.; Legon, A.C.; Marquardt, R.; Metrangolo, P.; Politzer, P.; Resnati, G.; Rissanen, K. Definition of the halogen bond (IUPAC Recommendations 2013). *Pure Appl. Chem.* **2013**, *85*, 1711–1713. [CrossRef]

88. McKinnon, J.J.; Jayatilaka, D.; Spackman, M.A. Towards quantitative analysis of intermolecular interactions with Hirshfeld surfaces. *Chem. Commun.* **2007**, *7*, 3814–3816. [CrossRef]

89. Alvarez, S. A cartography of the van der Waals territories. *Dalton Trans.* **2013**, *42*, 8617–8636. [CrossRef] [PubMed]

90. Cox, S.R.; Williams, D.E. Representation of the molecular electrostatic potential by a net atomic charge model. *J. Comput. Chem.* **1981**, *2*, 304–323. [CrossRef]

91. Politzer, P.; Lane, P.; Concha, M.C.; Ma, Y.; Murray, J.S. An overview of halogen bonding. *J. Mol. Model.* **2007**, *13*, 305–311. [CrossRef] [PubMed]

92. Politzer, P.; Murray, J.S.; Clark, T. Halogen bonding: An electrostatically-driven highly directional noncovalent interaction. *Phys. Chem. Chem. Phys.* **2010**, *12*, 7748–7757. [CrossRef] [PubMed]

93. Contreras-García, J.; Johnson, E.R.; Keinan, S.; Chaudret, R.; Piquemal, J.-P.; Beratan, D.N.; Yang, W. NCIPLOT: A Program for Plotting Noncovalent Interaction Regions. *J. Chem. Theory Comput.* **2011**, *7*, 625–632. [CrossRef] [PubMed]

94. Lefebvre, C.; Rubez, G.; Khartabil, H.; Boisson, J.-C.; Contreras-García, J.; Hénon, E. Accurately extracting the signature of intermolecular interactions present in the NCI plot of the reduced density gradient versus electron density. *Phys. Chem. Chem. Phys.* **2017**, *19*, 17928–17936. [CrossRef]

95. Becke, A.D.; Edgecombe, K.E. A simple measure of electron localization in atomic and molecular systems. *J. Phys. Chem.* **1990**, *92*, 5397–5403. [CrossRef]

96. Silvi, B.; Savin, A. Classification of chemical bonds based on topological analysis of electron localization functions. *Nature* **1994**, *371*, 683–686. [CrossRef]

97. Savin, A.; Nesper, R.; Wengert, S.; Fässler, T.F. ELF: The Electron Localization Function. *Angew. Chem. Int. Ed.* **1997**, *36*, 1808–1832. [CrossRef]

98. Espinosa, E.; Molins, E.; Lecomte, C. Hydrogen bond strengths revealed by topological analyses of experimentally observed electron densities. *Chem. Phys. Lett.* **1998**, *285*, 170–173. [CrossRef]

99. Vener, M.V.; Egorova, A.N.; Churakov, A.V.; Tsirelson, V.G. Intermolecular hydrogen bond energies in crystals evaluated using electron density properties: DFT computations with periodic boundary conditions. *J. Comput. Chem.* **2012**, *33*, 2303–2309. [CrossRef] [PubMed]

100. Bartashevich, E.V.; Tsirelson, V.G. Interplay between non-covalent interactions in complexes and crystals with halogen bonds. *Russ. Chem. Rev.* **2014**, *83*, 1181–1203. [CrossRef]

101. Malenov, D.P.; Janjić, G.V.; Medaković, V.B.; Hall, M.B.; Zarić, S.D. Noncovalent bonding: Stacking interactions of chelate rings of transition metal complexes. *Coord. Chem. Rev.* **2017**, *345*, 318–341. [CrossRef]

102. Ninković, D.B.; Blagojević Filipović, J.P.; Hall, M.B.; Brothers, E.N.; Zarić, S.D. What Is Special about Aromatic–Aromatic Interactions? Significant Attraction at Large Horizontal Displacement. *ACS Cent. Sci.* **2020**, *6*, 420–425. [CrossRef] [PubMed]

103. Bartashevich, E.; Yushina, I.; Kropotina, K.; Muhitdinova, S.; Tsirelson, V. Testing the tools for revealing and characterizing the iodine-iodine halogen bond in crystals. *Acta Crystallogr. B* **2017**, *73*, 217–226. [CrossRef] [PubMed]

104. Masaryk, L.; Moncol, J.; Herchel, R.; Nemec, I. Halogen Bonding in New Dichloride-Cobalt(II) Complex with Iodo Substituted Chalcone Ligands. *Crystals* **2020**, *10*, 354. [CrossRef]

105. Bulatova, M.; Ivanov, D.M.; Haukka, M. Classics Meet Classics: Theoretical and Experimental Studies of Halogen Bonding in Adducts of Platinum(II) 1,5-Cyclooctadiene Halide Complexes with Diiodine, Iodoform, and 1,4-Diiodotetrafluorobenzene. *Cryst. Growth Des.* **2021**, *21*, 974–987. [CrossRef]

106. Eliseeva, A.A.; Ivanov, D.M.; Rozhkov, A.V.; Ananyev, I.V.; Frontera, A.; Kukushkin, V.Y. Bifurcated Halogen Bonding Involving Two Rhodium(I) Centers as an Integrated σ-Hole Acceptor. *JACS Au* **2021**, *1*, 354–361. [CrossRef]

107. Mata, I.; Molins, E.; Alkorta, I.; Espinosa, E. Topological Properties of the Electrostatic Potential in Weak and Moderate N···H Hydrogen Bonds. *J. Phys. Chem. A* **2007**, *111*, 6425–6433. [CrossRef] [PubMed]

108. Zhao, N.; Wu, Y.-H.; Luo, J.; Shi, L.-X.; Chen, Z.-N. Aggregation-induced phosphorescence of iridium(iii) complexes with 2,2′-bipyridine-acylhydrazone and their highly selective recognition to Cu^{2+}. *Analyst* **2013**, *138*, 894–900. [CrossRef] [PubMed]

109. Kalinowski, J.; Cocchi, M.; Murphy, L.; Williams, J.A.G.; Fattori, V. Bi-molecular emissive excited states in platinum (II) complexes for high-performance organic light-emitting diodes. *Chem. Phys.* **2010**, *378*, 47–57. [CrossRef]

110. Diez, A.; Forniés, J.; Larraz, C.; Lalinde, E.; López, J.A.; Martín, A.; Moreno, M.T.; Sicilia, V. Structural and luminescence studies on pi...pi and Pt...Pt interactions in mixed chloro-isocyanide cyclometalated platinum(II) complexes. *Inorg Chem.* **2010**, *49*, 3239–3251. [CrossRef] [PubMed]

111. Díez, Á.; Forniés, J.; Fuertes, S.; Lalinde, E.; Larraz, C.; López, J.A.; Martín, A.; Moreno, M.T.; Sicilia, V. Synthesis and Luminescence of Cyclometalated Compounds with Nitrile and Isocyanide Ligands. *Organometallics* **2009**, *28*, 1705–1718. [CrossRef]

112. Kui, S.C.; Hung, F.-F.; Lai, S.-L.; Yuen, M.-Y.; Kwok, C.-C.; Low, K.-H.; Chui, S.S.-Y.; Che, C.-M. Luminescent organoplatinum(II) complexes with functionalized cyclometalated CˆNˆC ligands: Structures, photophysical properties, and material applications. *Chemistry* **2012**, *18*, 96–109. [CrossRef]